# A FRACTIONAL STUDY OF MHD CASSON FLUID MOTION WITH THERMAL RADIATIVE FLUX AND HEAT INJECTION/SUCTION MECHANISM UNDER RAMPED WALL CONDITION: APPLICATION OF RABOTNOV EXPONENTIAL KERNEL

**Aziz Ur REHMAN\*** , **Fahd JARAD\*\*/\*\*\*** , **Muhammad Bilal RIAZ\*/\*\*\*\***


\*Department of Mathematics, University of Management and Technology Lahore, Pakistan
\*\*Department of Mathematics, Cankaya University, Etimesgut 06790, Ankara, Turkey
\*\*\*Department of Medical Research, China Medical University, Taichung 40402, Taiwan
\*\*\*\*Department of Computer Science and Mathematics, Lebanese American University, Byblos, Lebanon

prof.azizkhan@gmail.com, fahd@cankaya.edu.tr, bilal.riaz@umt.edu.pk

**Abstract:** The primary objective of this research is to extend the concept of fractionalized Casson fluid flow. In this study, a comprehensive analysis of magnetohydrodynamic (MHD) natural convective flow of Casson fluid is conducted, focusing on obtaining analytical solutions using the non-integer-order derivative known as the Yang–Abdel-Aty–Cattani (YAC) operator. The YAC operator utilized in this research possesses a more generalized exponential kernel. The fluid flow is examined in the vicinity of an infinitely vertical plate with a characteristic velocity denoted as $u_0$. The mathematical modelling of the problem incorporates partial differential equations, incorporating Newtonian heating and ramped conditions. To facilitate the analysis, a suitable set of variables is introduced to transform the governing equations into a dimensionless form. The Laplace transform (LT) is then applied to the fractional system of equations, and the obtained results are presented in series form and also expressed in terms of special functions. The study further investigates the influence of relevant parameters, such as $\alpha$, $\beta$, $P_r$, $Q$, $G_r$, $M$, $N_r$ and $K$, on the fluid flow to reveal interesting findings. A comparison of different approaches reveals that the YAC method yields superior results compared to existing operators found in the literature. Graphs are generated to illustrate the outcomes effectively. Additionally, the research explores the limiting cases of the Casson and viscous fluid models to derive the classical form from the YAC fractionalized Casson fluid model.

**Key words:** YAC derivative, series solution, heat transfer, Laplace transformation, Rabotnov exponential functions, system parameters

## 1. INTRODUCTION

Non-Newtonian fluids have gained significant importance among researchers and scientists in recent decades due to their wide range of applications in various fields. The complex nature of these fluids prevents the characterization of their mechanical properties using the Navier–Stokes equation, making a single constitutive equation inadequate for describing their rheological behaviour. The rheological behaviour of non-Newtonian fluids is of great significance in industrial and technological applications, such as petroleum, biological, plastic manufacturing, chemical, textile and cosmetic industries. Several models, including the viscoplastic model, second-grade fluid model, Williamson fluid, Bingham plastic model, power law model, Jeffery model, Brinkman type fluid, Oldroyd-B model, Maxwell model, Walters-B fluid model, tangent hyperbolic fluid and Casson model (shear thinning liquid), have been developed to explain the diverse nature of non-Newtonian fluids [1–6].

Among these models, the Casson fluid is considered the simplest generalization of a Newtonian fluid. Casson fluid, introduced by Casson in 1959 to analyse the regime of pigment-oil suspensions, is one of the most common types of non-Newtonian fluids [7]. The Casson fluid model allows for the determination of viscous fluid behaviour by considering the impacts of its generalized

parameters. Due to its important properties and wide range of applications, Casson fluid finds application in biological sciences, such as plasma and the handling of biological fluids like blood, as well as in mechanics due to its viscoelastic behaviour. Given the current scientific challenges, mathematicians, researchers, scientists and engineers are particularly focused on studying Casson fluid in fields like biology, engineering, chemistry, petroleum industries and physiology, considering its natural behaviour. Hussain et al. [8] employed the Homotopy analysis method, an analytical technique, to investigate series solutions for magneto-hydrodynamic (MHD) Casson fluid in the thermal boundary layer flow over a moving stretching porous wedge. Additionally, Hussain et al. [9] discussed the solution of the MHD thermal boundary layer flow of Casson liquid over a penetrable extending wedge with ohmic heating and convective boundary conditions.

Ramped conditions refer to a flow condition where the shear rate of a fluid gradually changes over time. This approach is commonly employed in the investigation of non-Newtonian fluids to gain insights into their flow behaviour and properties under different circumstances. In the pharmaceutical industry, ramped conditions are utilized to study the rheological behaviour of complex fluids like suspensions and emulsions, which often exhibit non-Newtonian characteristics. The application of ramped conditions extends to the oil and gas industry, where they are employed

to model the flow of non-Newtonian fluids. Understanding the rheological behaviour of drilling mud and other fluids is crucial for optimizing drilling operations. In the field of biomedical engineering, ramped conditions are used to study blood flow in arteries and veins. The behaviour of non-Newtonian fluids plays a critical role in comprehending the pathophysiology of diseases such as atherosclerosis. Ali et al. [10] developed a mathematical model to examine blood flow through a cylindrical stenosed blood vessel. Overall, ramped conditions have significant applications in the study of non-Newtonian fluids. They enable researchers to gain a better understanding of the flow behaviour of these fluids under various conditions, which is essential for optimizing their performance in diverse applications. Khalid et al. [11] investigated the MHD unsteady free convectional transport of the Casson model, considering computational aspects in porous media. Hussain et al. [12] discussed the effects of chemical reactions and suction/injection on the flow of Williamson fluid along a porous stretching wedge. Bhattacharyya et al. [13] described the MHD flow of Casson fluid velocity in the presence of an exponentially stretching surface. Oka [14] conducted the first-time analysis of Casson fluid movement, considering convective conditions at the boundary through a permeable stretching sheet, and analysed the results theoretically. Riaz et al. [15] investigated the impacts of heat generation on MHD Maxwell fluid in a permeable medium. Hussain et al. [16] analyzed the flow of a hybrid nanofluid under the influence of MHD, variable viscosity and mixed convection. Mernone et al. [17] examined the two-dimensional peristaltic flow of Casson fluid in a channel. Arthur et al. [18] investigated the generalized peristaltic flow of Casson fluid in a permeable channel subjected to chemical reaction effects. Mukhopadhyay [19] examined the heat transfer phenomenon of MHD Casson fluid with heat suction/blowing passing over a stretching plate. Mustafa et al. [20] analysed the unsteady flow of the Casson model using the homotopy analysis method to study heat transfer over a movable flat plate. Similar studies on MHD Casson fluid can be found in the literature [21–23] and references therein.

Fractional calculus has diverse and significant impacts in various fields such as electrical engineering, electrochemistry, control theory, electromagnetism, mechanics, image processing, bioengineering, physics, finance and fluid dynamics. It is a valuable tool for research and study due to its wide-ranging applications. Fractional derivatives not only capture the present behaviour of systems but also account for their past behaviour, making them particularly suitable for systems with long-term memory. Its applications extend beyond physical sciences to areas like biology, astrophysics, ecology, geology and chemistry. In the past decades, fractional calculus has successfully elucidated the mechanisms of non-Newtonian models by providing a simple and elegant description of their complex behaviour. One well-known type of non-Newtonian fluid is viscoelastic fluid, which exhibits both elasticity and viscosity. These fluid models have significant implications in polymerization, industrial and mechanical engineering, as well as the automobile industry, due to their inherent characteristics. Fractional calculus plays a crucial role in interpreting the viscoelastic nature of materials. Given these remarkable properties, researchers have dedicated attention to analysing the fractional behaviour of different fluid models, either directly or indirectly, particularly when considering non-integer-order derivatives. For example, Kumar et al. [24] illustrated the multidimensional heat equations of arbitrary order using the analytical approaches of the homotopy perturbation transform method (HPTM) and residual power series method, employing a new fractional operator in the Yang–Abdel-Aty–Cattani (YAC) sense. Bagley and Torvik [25] explored the application of fractional calculus to viscoelastic fluids. Rehman et al. [26] investigated the fractional Maxwell fluid and obtained closed solutions for shear stress and velocity. Riaz et al. [27] analysed the influence of MHD on the heat transfer of fractionalized Oldroyd-B fluid. Additionally, Rehman et al. [28] studied certain features of Maxwell fluid, considering the impact of Newtonian heating and developed a fractional model using the Prabhakar fractional approach. Mohammadi et al. [29] utilized the Euler method for fractional-order Caputo Fabrizio derivative to approximate the system's solution and analyse the effects of the mumps virus. Rehman et al. [30] performed a comparative analysis of ABC, CF and CPC methods for a second-grade fluid under the influence of Newtonian heating, obtaining series solutions. Kumar et al. [31] proposed a new generalized fractional derivative that produces different types of singular and nonsingular fractional derivatives based on various kernels. Jleli et al. [32] presented a general framework of the HPTM for the analytic treatment of time-fraction partial differential equations following the YAC approach. Furthermore, Hayat et al. [33] obtained a series solution for the flow of Jeffery fluid, highlighting the contributions of fractional calculus to viscoelastic fluids in various studies [34–39].

In a recent study, Anwar et al. [40] investigated the classical version of the Casson fluid model with ramped boundary conditions using the Laplace transformation method. This method is efficient for non-uniform boundary conditions, but it does not consider the fractional behaviour effect in the presented model. It was observed that the Casson fluid model with the innovative fractional operator, known as the YAC operator, which has a non-local and singular kernel, has not been previously studied in conjunction with ramped boundary conditions for velocity and energy distribution through porous media in the literature on fractional models in fluid mechanics. Motivated by these findings, this article focuses on the heat transfer analysis of the MHD fractional Casson fluid in a channel with ramped conditions. The integer-order derivative Casson fluid model is transformed into the non-integer-order derivative YAC model. The Laplace transform (LT) is used to obtain analytical solutions for the problem at hand. The velocity and temperature are evaluated in series form, providing exact solutions that have not been reported in the previous literature. Therefore, this article contributes valuable insights to the existing literature by presenting a wide range of exact solutions for the Casson fluid with appropriate boundary conditions. The influence of embedded parameters, including the YAC fractional parameter $\alpha$, porosity parameter $\mathrm{K}$, Casson fluid parameter $\beta$, Prandtl parameter $\mathrm{P_r}$, magnetic number $\mathrm{M}$, heat injection/suction parameter $\mathrm{Q}$, Grashof number $\mathrm{G_r}$ and radiation parameter $\mathrm{N_r}$, on the velocity profile and heat distribution, are analysed using graphical representations.

## 2. MATHEMATICAL MODEL

In this study, we investigate the heat transfer phenomenon in the convective flow of an MHD Casson fluid over a vertically oriented infinite plate. The coordinate axis system is set up such that the plate is fixed along the x-axis, and the ∅-axis is perpendicular to the plate (as depicted in Fig. 1). Initially, at time $t = 0$, the fluid is at rest with the ambient temperature $T_\infty$. Ramped conditions are applied to the velocity for $t > 0$, with the wall temperature set as $T_w$.
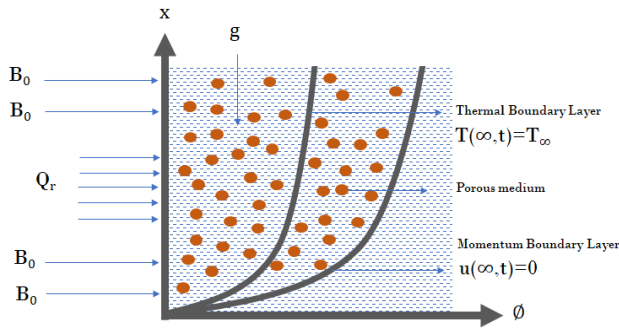
**Fig. 1.** Schematic drawing of the flow model

The velocity component $u(\varphi, t)$ is considered along the x-axis, where $u_0$ represents the characteristic velocity, and the fluid flow is confined to $\varphi > 0$. We make certain assumptions in our model. First, a vertical transverse magnetic force is introduced and exerted on the fluid flow, and the fluid motion is assumed to be unidirectional. We neglect the influence of the induced magnetic field due to the small value of the Reynolds parameter/number. Viscous dissipation, Joule heating, radiative heat flux ($Q_r$) and any other external heat sources are also disregarded. Additionally, we assume that the fluid velocity in this problem is only dependent on the two parameters, $\varphi$ and t. Under these assumptions, the governing equations for the fluid flow, using Boussinesq's approximation [41, 42], can be expressed as follows:

The following equations represent the momentum and energy equations:

$$\frac{\partial u(\varphi, t)}{\partial t} = v\left(1 + \frac{1}{\beta}\right)\frac{\partial^2 u(\varphi, t)}{\partial \varphi^2} + g\beta_T(T(\varphi, t) - T_\infty)$$
$$- \frac{\sigma}{\rho}B_0^2 u(\varphi, t) - v\left(1 + \frac{1}{\beta}\right)\frac{\zeta}{k_p}u(\varphi, t), \tag{1}$$

$$\rho C_p \frac{\partial T(\varphi, t)}{\partial t} = -\frac{\partial q(\varphi, t)}{\partial \varphi} - \frac{\partial Q_r}{\partial \varphi} + Q_0(T(\varphi, t) - T_\infty), \tag{2}$$

where

$$\left[Q_r = -\frac{4\sigma_1}{3k_1}\frac{\partial T^4}{\partial \varphi}; T^4 \approx 4T_\infty^3 T - 3T_\infty^4\right].$$

Fourier's Law of thermal flux is written as

$$q(\varphi, t) = -k\frac{\partial T(\varphi, t)}{\partial \varphi}. \tag{3}$$

The mathematical representation of the given problem, including the associated initial conditions and ramped boundary conditions, is presented as follows:

$$u(\varphi, 0) = 0, \quad T(\varphi, 0) = T_\infty, \quad \varphi \geq 0,$$

$$u(0, t) = \begin{cases} u_0\frac{t}{t_0}, & 0 < t \leq t_0; \\ u_0, & t > t_0 \end{cases},$$

$$T(0, t) = \begin{cases} T_\infty + (T_w - T_\infty)\frac{t}{t_0}, & 0 < t \leq t_0; \\ T_w, & t > t_0 \end{cases},$$

$$u(\varphi, t) \to 0, T(\varphi, t) \to T_\infty, \text{ as } \varphi \to \infty \text{ and } t > 0. \tag{4}$$

A new set of quantities is introduced to non-dimensionalise the problem equations. This allows for a more convenient representation of the equations without specific units. By utilizing these non-dimensional quantities, the problem can be analysed and compared across different scales or systems.

$$t^* = \frac{u_0^2 t}{v}, \quad \varphi^* = \frac{u_0\varphi}{v}, \quad u^* = \frac{u}{u_0}, \quad q^* = \frac{q}{q_0}, \quad T^* = \frac{T-T_\infty}{T_w-T_\infty},$$

$$q_0 = \frac{k(T_w-T_\infty)u_0}{v}, Q = \frac{Q_0 v}{\rho C_p u_0^2}, Gr = \frac{g\beta_T(T_w-T_\infty)}{u_0^3},$$

$$Pr = \frac{\mu C_p}{k}, M = \frac{\sigma B_0^2 v}{\rho u_0^2}, N_r = \frac{16\sigma_1 T_\infty^3}{3kK_1}, \frac{1}{K} = \frac{v^2\zeta}{k_p u_0^2}. \tag{5}$$

Upon substituting the newly introduced entities, as defined in Eq. (5), into Eqs (1) and (2), and subsequently omitting the $*$ symbol, the equations undergo a transformation that results in a revised form. This process involves replacing the relevant variables or terms with their corresponding values based on the definitions provided in Eq. (5).

By applying these substitutions and simplifications, the equations are modified to better represent the desired form or structure, allowing for clearer mathematical expressions and further analysis. The specific details of the transformations depend on the specific equations and substitutions involved, as well as the context in which they are applied.

$$\frac{\partial u(\varphi, t)}{\partial t} = b\frac{\partial^2 u(\varphi, t)}{\partial \varphi^2} - \left[M + \frac{b}{K}\right]u(\varphi, t) + GrT(\varphi, t), \tag{6}$$

$$\frac{\partial T(\varphi, t)}{\partial t} = -\left(\frac{1+Nr}{Pr}\right)\frac{\partial q(\varphi, t)}{\partial \varphi} + QT, \tag{7}$$

$$q(\varphi, t) = -\frac{\partial T(\varphi, t)}{\partial \varphi}. \tag{8}$$

The non-dimensional forms of the initial and boundary conditions are also considered in this context

$$u(\varphi, 0) = 0, \quad T(\varphi, 0) = 0, \text{for } \varphi \geq 0, \tag{9}$$

$$u(0, t) = T(0, t) = \begin{cases} t & 0 < t \leq 1 \\ 1 & t > 1 \end{cases}, \tag{10}$$

$$u(\varphi, t) \to 0, \quad T(\varphi, t) \to 0 \text{ as } \varphi \to \infty \text{ and } t > 0, \tag{11}$$

where

$$a = b\theta Q + c, b = 1 + \frac{1}{\beta}, c = M + \frac{b}{K}, d = 1 - b\theta, \theta = \frac{Pr}{1+N_r}.$$

In this context, the term Grashof number is used to represent the parameter $G_r$, the Prandtl number is denoted by $P_r$, the radiation parameter is represented by $N_r$, the magnetic number is denoted as _M,_ permeability is represented by $k_p$, thermal conductivity is denoted by _k_, the coefficient of Rossland absorption is denoted by $k_1$, the Stefan–Boltzmann constant is represented by $ó_1$, porosity is denoted by $\xi$, radiative heat flux is represented by $Q_r$ and porosity is defined as _K_.

## 3. PRELIMINARIES

In this article, the non-integer YAC time derivative is applied which is defined as

$$^{YAC}D_t^\alpha f(t) = \int_0^t \Psi_\alpha\left(-\wp(t - \tau)^\alpha\right)f'(\tau)d\tau, \tag{12}$$

for $t > 0, 0 < \alpha < 1$,

where

$$\Psi(\wp z^\alpha) = \sum_{n=0}^\infty \frac{\wp^n z^{(n+1)(\alpha+1)-1}}{\Gamma(n+1)(\alpha+1)}, \quad z \in \mathbb{C},$$

and $\Psi_\alpha$ denotes the Rabotnov exponential function of order $\alpha$.

Laplace transformation of this newly developed operator is defined as follows:

$$L\{YACD_t^\alpha f(t)\} = \frac{1}{\eta^{\alpha+1}} \frac{\eta L\{f(t)\} - f(0)}{1 + \wp \eta^{-(\alpha+1)}}, \tag{13}$$

where $\eta$ represents LT parameter and $\alpha$ used as a fractional parameter.

## 4. FRACTIONAL FORMULATION OF GOVERNING EQUATIONS AND SOLUTIONS

By replacing the regular time derivative with the YAC fractional derivative in Eqs. (6)–(8), the modified equations for the time-fractional rate-type fluid model describing velocity and energy are obtained. This substitution allows for a more accurate representation of fractional behaviour, as the YAC fractional derivative incorporates non-local and singular kernels. Hence, the resulting equations provide a comprehensive framework for understanding the dynamics of the fluid in terms of velocity and energy within the context of a time-fractional rate-type fluid model.

$$^{YAC}D_t^\alpha u(\varphi, t) = b\frac{\partial^2 u(\varphi,t)}{\partial \varphi^2} - cu(\varphi,t) + GrT(\varphi,t), \tag{14}$$

$$^{YAC}D_t^\alpha T(\varphi, t) = \frac{1}{\theta}\frac{\partial^2 T(\varphi,t)}{\partial \varphi^2} + QT(\varphi,t). \tag{15}$$

The YAC fractional operator, denoted as $^{YAC}D_t^\alpha$, is utilized in the context mentioned above. More details regarding the properties of the YAC operator can be found in the study referenced as [43].

### 4.1. Investigation of exact solution for temperature profile

By applying the LT to Eq. (15) while considering the transformed conditions specified in Eqs (9)–(11), we obtain

$$\frac{\eta\bar{T}(\varphi,\eta) - \bar{T}(\varphi,0)}{\eta^{\alpha+1}+\wp} = \frac{1}{\theta}\frac{\partial^2\bar{T}(\varphi,\eta)}{\partial\varphi^2} + Q\bar{T}(\varphi,\eta). \tag{16}$$

With transformed boundary conditions

$$\bar{T}(\varphi,0) = 0, \quad \bar{T}(0,\eta) = \frac{1-e^{-\eta}}{\eta^2}$$

and $\bar{T}(\varphi,\eta) \to 0$ as $\varphi \to \infty$. (17)

By applying the Laplace transformation to Eq. (16), the solution for the energy can be derived as follows:

$$\bar{T}(\varphi,\eta) = e_1 e^{-\varphi\sqrt{\theta\left(\frac{\eta}{\eta^{\alpha+1}+\wp}-Q\right)}} + e_2 e^{\varphi\sqrt{\theta\left(\frac{\eta}{\eta^{\alpha+1}+\wp}-Q\right)}}. \tag{18}$$

After implementing the transformed boundary conditions, the energy solution can be expressed as follows:

$$\bar{T}(\varphi,\eta) = \left(\frac{1-e^{-\eta}}{\eta^2}\right)e^{-\varphi\sqrt{\theta\left(\frac{\eta}{\eta^{\alpha+1}+\wp}-Q\right)}}, \tag{19}$$

$$= \overline{T_1}(\varphi,\eta) - e^{-\eta}\overline{T_1}(\varphi,\eta).$$

To transform the solution in time variable again, we have to employ inverse Laplace transformation technique on Eq. (19).

$$T(\varphi,t) = T_1(\varphi,t) - T_1(\varphi,t)P(t-1). \tag{20}$$

In the above expression, $P(t-1)$ represents a Heaviside function and

$$T_1(\varphi,t) = \text{盎} \tag{21}$$

The current form of Eq. (21) makes it challenging to compute the Laplace inverse. Therefore, it is necessary to convert it into a series form, which will yield the following expression:

$$T_1(\varphi,t) = L^{-1}\left\{\frac{1}{\eta^2}\sum_{\chi=0}^\infty\sum_{n=0}^\infty\frac{(-\varphi)^\chi(\theta)^{\frac{\chi}{2}}(-Q)^{\frac{\chi}{2}-n}\Gamma(\frac{\chi}{2}+1)(\eta)^n}{\chi!n!\Gamma(\frac{\chi}{2}-n+1)(\eta^{\alpha+1}+\wp)^n}\right\},$$

$$= \sum_{\chi=0}^\infty\sum_{n=0}^\infty\frac{(-\varphi)^\chi(\theta)^{\frac{\chi}{2}}(-Q)^{\frac{\chi}{2}-n}\Gamma(\frac{\chi}{2}+1)}{\chi!n!\Gamma(\frac{\chi}{2}-n+1)}t^{n\alpha+1}E_{\alpha+1,n\alpha+2}^n(-\wp t^{\alpha+1}),$$

by using $L^{-1}\left\{\frac{\eta^{\alpha\gamma-\beta}}{(\eta^\alpha-\wp)^\gamma}\right\} = t^{\beta-1}E_{\alpha,\beta}^\gamma(\wp t^\alpha)$.

### 4.2. Investigation of exact solution for fluid velocity

Applying the Laplace transformation into Eq. (14) with appropriate transformed conditions as defined in Eqs. (9)–(11), we get

$$\frac{\eta\bar{u}(\varphi,\eta) - \bar{u}(\varphi,0)}{\eta^{\alpha+1}+\wp} = b\frac{d^2\bar{u}(\varphi,\eta)}{d\varphi^2} - c\bar{u}(\varphi,\eta) + Gr\bar{T}(\varphi,\eta), \tag{22}$$

with conditions are

$$\bar{u}(\varphi,0) = 0, \quad \bar{u}(0,\eta) = \frac{1-e^{-\eta}}{\eta^2}$$

and $\bar{u}(\varphi,\eta) \to 0$ as $\varphi \to \infty$. (23)

By substituting the computed temperature $\bar{T}(\varphi,\eta)$ obtained from Eq. (19) into Eq. (22), the resulting solution can be expressed in a simplified form as follows:

$$\bar{u}(\varphi,\eta) = e_5 e^{-\varphi\sqrt{\frac{1}{b}\left(\frac{\eta}{\eta^{\alpha+1}+\wp}+c\right)}} + e_6 e^{\varphi\sqrt{\frac{1}{b}\left(\frac{\eta}{\eta^{\alpha+1}+\wp}+c\right)}}$$

$$+ Gr\left(\frac{1-e^{-\eta}}{\eta^2}\right)\frac{e^{-\varphi\sqrt{\theta\left(\frac{\eta}{\eta^{\alpha+1}+\wp}-Q\right)}}}{a+\frac{d\eta}{\eta^{\alpha+1}+\wp}}. \tag{24}$$

By utilizing the transformed boundary conditions, we can ascertain the unknown constant. Subsequently, the solution for the velocity in Eq. (24) can be expressed as follows:

$$\bar{u}(\varphi,\eta) = \left(\frac{1-e^{-\eta}}{\eta^2}\right)e^{-\varphi\sqrt{\frac{1}{b}\left(\frac{\eta}{\eta^{\alpha+1}+\wp}+c\right)}}$$

$$+ \frac{Gr(1-e^{-\eta})}{\eta^2\left(a+\frac{d\eta}{\eta^{\alpha+1}+\wp}\right)}\left[e^{-\varphi\sqrt{\theta\left(\frac{\eta}{\eta^{\alpha+1}+\wp}-Q\right)}} - e^{-\varphi\sqrt{\frac{1}{b}\left(\frac{\eta}{\eta^{\alpha+1}+\wp}+c\right)}}\right]. \tag{25}$$

To find Laplace inverse of Eq. (25), first we write it in the following form:

$$\bar{u}(\varphi,\eta) = \bar{\Omega}(\varphi,\eta) + Gr\bar{\Phi}(\varphi,\eta)[\bar{T}(\varphi,\eta) - \bar{\Omega}(\varphi,\eta)] \tag{26}$$

and

$$\bar{\Omega}(\varphi,\eta) = \overline{\Omega_1}(\varphi,\eta) - e^{-\eta}\overline{\Omega_1}(\varphi,\eta). \tag{27}$$

The inverse Laplace of Eq. (27) is obtained as

$$\Omega(\varphi,t) = \Omega_1(\varphi,t) - \Omega_1(\varphi,t)P(t-1), \tag{28}$$

where

Aziz Ur Rehman, Fahd Jarad, Muhammad Bilal Riaz
*A Fractional Study of MHD Casson Fluid Motion with Thermal Radiative Flux and Heat Injection/Suction Mechanism under Ramped Wall Condition:*
*Application of Rabotnov Exponential Kernel*

DOI 10.2478/ama-2024-0011

$$\Omega_1(\varphi,t) = L^{-1}\{\overline{\Omega_1}(\varphi,\eta)\} = L^{-1}\left\{\frac{1}{\eta^2}e^{-\varphi\sqrt{\frac{1}{b}\left(\frac{\eta}{\eta^{\alpha+1}+\wp}+c\right)}}\right\},$$

$$= L^{-1}\left\{\frac{1}{\eta^2}\sum_{\chi=0}^{\infty}\sum_{n=0}^{\infty}\frac{(-\varphi)^\chi(c)^{\frac{\chi}{2}-n}\Gamma(\frac{\chi}{2}+1)(\eta)^n}{\chi!n!(b)^{\frac{\chi}{2}}\Gamma(\frac{\chi}{2}-n+1)(\eta^{\alpha+1}+\wp)^n}\right\},$$

$$= \sum_{\chi=0}^{\infty}\sum_{n=0}^{\infty}\frac{(-\varphi)^\chi(c)^{\frac{\chi}{2}-n}\Gamma(\frac{\chi}{2}+1)}{\chi!n!(b)^{\frac{\chi}{2}}\Gamma(\frac{\chi}{2}-n+1)}t^{n\alpha+1}E_{\alpha+1,n\alpha+2}^n(-\wp t^{\alpha+1}),$$

$$\Phi(\varphi,t) = L^{-1}\{\overline{\Phi}(\varphi,\eta)\} = L^{-1}\left\{\frac{1}{a+\frac{d\eta}{\eta^{\alpha+1}+\wp}}\right\},$$

$$= L^{-1}\left\{\sum_{m=0}^{\infty}\frac{(-1)^m(d)^m(\eta)^m}{(a)^{m+1}(\eta^{\alpha+1}+\wp)^m}\right\},$$

$$= \sum_{m=0}^{\infty}\frac{(-1)^m(d)^m}{(a)^{m+1}}t^{m\alpha-1}E_{\alpha+1,m\alpha}^m(-\wp t^{\alpha+1}).$$

The required velocity solution after employing the definition of inverse Laplace operator in Eq. (26) is

$$u(\varphi,t) = \Omega(\varphi,t) + Gr\Phi(\varphi,t)*[T(\varphi,t)-\Omega(\varphi,t)]. \quad (29)$$

### 4.3. Limiting models

This section focuses on specific cases that arise when certain physical parameters are not present. These cases provide an opportunity to examine the influence of different circumstances on the solutions. By exploring these scenarios, we can gain valuable insights into the system's behaviour and characteristics when specific parameters are disregarded. This analysis contributes to a holistic understanding of the problem and deepens our knowledge of its dynamics.

#### 4.3.1 Solution in the absence of Casson parameter

In this case, let us assume that the Casson fluid parameter, denoted as $\beta$, is chosen to be extremely large, meaning $1/\beta \to 0$. After this transformation, the velocity field solution of the newly derived viscous fluid, obtained from the previously calculated velocity Eq. (25), can be expressed as

$$\bar{u}(\varphi,\eta) = \left(\frac{1-e^{-\eta}}{\eta^2}\right)e^{-\varphi\sqrt{\left(\frac{\eta}{\eta^{\alpha+1}+\wp}+c_1\right)}}$$
$$+\frac{Gr(1-e^{-\eta})}{\eta^2\left(a_1+\frac{d_1\eta}{\eta^{\alpha+1}+\wp}\right)}\left[e^{-\varphi\sqrt{\theta\left(\frac{\eta}{\eta^{\alpha+1}+\wp}-Q\right)}}-e^{-\varphi\sqrt{\left(\frac{\eta}{\eta^{\alpha+1}+\wp}+c_1\right)}}\right], \quad (30)$$

where $a_1 = \theta Q + c_1$, $c_1 = M + \frac{1}{K}$, $d_1 = 1 - \theta$.

To find Laplace inverse of Eq. (30), first we write it in the following form:

$$\bar{u}(\varphi,\eta) = \bar{\omega}(\varphi,\eta) + Gr\overline{\Psi}(\varphi,\eta)[\overline{T}(\varphi,\eta)-\bar{\omega}(\varphi,\eta)] \quad (31)$$

and

$$\overline{\omega}(\varphi,\eta) = \overline{\omega_1}(\varphi,\eta) - e^{-\eta}\overline{\omega_1}(\varphi,\eta). \quad (32)$$

After the application of Laplace inverse operator, Eq. (32) is turn out again in the time variable as

$$\omega(\varphi,t) = \omega_1(\varphi,t) - \omega_1(\varphi,t)P(t-1), \quad (33)$$

where

$$\omega_1(\varphi,t) = L^{-1}\{\overline{\omega_1}(\varphi,\eta)\} = L^{-1}\left\{\frac{1}{\eta^2}e^{-\varphi\sqrt{\left(\frac{\eta}{\eta^{\alpha+1}+\wp}+c_1\right)}}\right\},$$

$$= L^{-1}\left\{\frac{1}{\eta^2}\sum_{\chi=0}^{\infty}\sum_{n=0}^{\infty}\frac{(-\varphi)^\chi(c_1)^{\frac{\chi}{2}-n}\Gamma(\frac{\chi}{2}+1)(\eta)^n}{\chi!n!\Gamma(\frac{\chi}{2}-n+1)(\eta^{\alpha+1}+\wp)^n}\right\},$$

$$= \sum_{\chi=0}^{\infty}\sum_{n=0}^{\infty}\frac{(-\varphi)^\chi(c_1)^{\frac{\chi}{2}-n}\Gamma(\frac{\chi}{2}+1)}{\chi!n!\Gamma(\frac{\chi}{2}-n+1)}t^{n\alpha+1}E_{\alpha+1,n\alpha+2}^n(-\wp t^{\alpha+1}),$$

$$\Psi(\varphi,t) = L^{-1}\{\overline{\Psi}(\varphi,\eta)\} = L^{-1}\left\{\frac{1}{a_1+\frac{d_1\eta}{\eta^{\alpha+1}+\wp}}\right\},$$

$$= L^{-1}\left\{\sum_{m=0}^{\infty}\frac{(-1)^m(d_1)^m(\eta)^m}{(a_1)^{m+1}(\eta^{\alpha+1}+\wp)^m}\right\},$$

$$= \sum_{m=0}^{\infty}\frac{(-1)^m(d_1)^m}{(a_1)^{m+1}}t^{m\alpha-1}E_{\alpha+1,m\alpha}^m(-\wp t^{\alpha+1}).$$

The inverse Laplace of Eq. (31), the required velocity field solution, is finally written as

$$u(\varphi,t) = \omega(\varphi,t) + Gr\Psi(\varphi,t)*[T(\varphi,t)-\omega(\varphi,t)]. \quad (34)$$

#### 4.3.2 Solution in the absence of magnetic and porosity parameter

In this scenario, let us assume that $M = 0$ and $\frac{1}{K} = 0$ in the velocity equation (25), resulting in the following simplified form:

$$\bar{u}(\varphi,\eta) = \left(\frac{1-e^{-\eta}}{\eta^2}\right)e^{-\varphi\sqrt{\frac{1}{b}\left(\frac{\eta}{\eta^{\alpha+1}+\wp}\right)}}$$
$$+\frac{Gr(1-e^{-\eta})}{\eta^2\left(b\theta Q+\frac{d\eta}{\eta^{\alpha+1}+\wp}\right)}\left[e^{-\varphi\sqrt{\theta\left(\frac{\eta}{\eta^{\alpha+1}+\wp}-Q\right)}}-e^{-\varphi\sqrt{\frac{1}{b}\left(\frac{\eta}{\eta^{\alpha+1}+\wp}\right)}}\right]. \quad (35)$$

To find Laplace inverse of Eq. (35), first we write it in the following form:

$$\bar{u}(\varphi,\eta) = \overline{\Upsilon}(\varphi,\eta)$$
$$+Gr\overline{\varpi}(\varphi,\eta)[\overline{T}(\varphi,\eta)-\overline{\Upsilon}(\varphi,\eta)] \quad (36)$$

and

$$\overline{\Upsilon}(\varphi,\eta) = \overline{\Upsilon_1}(\varphi,\eta) - e^{-\eta}\overline{\Upsilon_1}(\varphi,\eta). \quad (37)$$

After the application of Laplace inverse operator, Eq. (37) is turn out again in the time variable as

$$\Upsilon(\varphi,t) = \Upsilon_1(\varphi,t) - \Upsilon_1(\varphi,t)P(t-1), \quad (38)$$

where

$$\Upsilon_1(\varphi,t) = L^{-1}\{\overline{\Upsilon_1}(\varphi,\eta)\} = L^{-1}\left\{\frac{1}{\eta^2}e^{-\varphi\sqrt{\frac{1}{b}\left(\frac{\eta}{\eta^{\alpha+1}+\wp}\right)}}\right\},$$

$$= L^{-1}\left\{\frac{1}{\eta^2}\sum_{\chi=0}^{\infty}\sum_{n=0}^{\infty}\frac{(-\varphi)^\chi\Gamma(\frac{\chi}{2}+1)(\eta)^n}{\chi!n!(b)^{\frac{\chi}{2}}\Gamma(\frac{\chi}{2}-n+1)(\eta^{\alpha+1}+\wp)^n}\right\},$$

$$= \sum_{\chi=0}^{\infty}\sum_{n=0}^{\infty}\frac{(-\varphi)^\chi\Gamma(\frac{\chi}{2}+1)}{\chi!n!(b)^{\frac{\chi}{2}}\Gamma(\frac{\chi}{2}-n+1)}t^{n\alpha+1}E_{\alpha+1,n\alpha+2}^n(-\wp t^{\alpha+1}),$$

$$\varpi(\varphi,t) = L^{-1}\{\overline{\varpi}(\varphi,\eta)\} = L^{-1}\left\{\frac{1}{b\theta Q+\frac{d\eta}{\eta^{\alpha+1}+\wp}}\right\},$$

$$= L^{-1}\left\{\sum_{m=0}^{\infty}\frac{(-1)^m(d)^m(\eta)^m}{(b\theta Q)^{m+1}(\eta^{\alpha+1}+\wp)^m}\right\},$$

$$= \sum_{m=0}^{\infty} \frac{(-1)^m (d)^m}{(b\theta Q)^{m+1}} t^{m\alpha-1} E_{\alpha+1,m\alpha}^m (-\wp t^{\alpha+1}).$$

The inverse Laplace of Eq. (36), the required velocity field solution, is finally written as

$$u(\varphi, t) = \Upsilon(\varphi, t) + Gr\varpi(\varphi, t) * [T(\varphi, t) - \Upsilon(\varphi, t)]. \quad (39)$$

## 5. RESULTS AND DISCUSSION

This study focuses on analysing the heat transfer in the natural convective flow of Casson fluid under the influence of MHD. The aim is to derive analytical solutions using the non-integer-order derivative YAC model. The fluid flow occurs along the $\varphi$-axis, and a dimensionless system of equations representing the phenomenon is solved using integral LT. The results obtained are presented in series form and also expressed in terms of special functions. To visually depict the effects of various physical parameters, such as the memory parameter ($\alpha$), Prandtl number ($P_r$), Casson parameter ($\beta$), heat absorption parameter ($Q$), thermal Grashof number ($G_r$), magnetic parameter ($M$), chemical reaction rate ($N_r$) and porosity parameter ($K$), graphical illustrations are utilized. Figs. 2–11 portray the velocity and temperature distribution of the Casson fluid under different parameter values using graphical software.
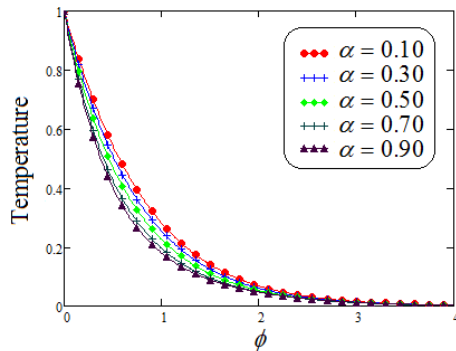


**Fig. 2.** Influence of Casson fluid temperature against $\varphi$ for multiple values of $\alpha$

Fig. 2 illustrates the influence of the memory parameter on the temperature profile. As the value of $\alpha$ increases, the boundary layer thickens, leading to a decrease in temperature. The validity of the obtained result can be easily confirmed by considering the limit as $\alpha \rightarrow 1$. The Prandtl number is a dimensionless quantity that characterizes the relative importance of momentum diffusion to thermal diffusion in a fluid. It provides valuable information about the rate of heat transfer and the thermal boundary layer in various fluid flow systems. The prevalence of mass diffusivity in fluid flow leads to a decrease in the thermal boundary layer, consequently causing a reduction in temperature. These effects, as demonstrated in Fig. 3, can be attributed to the influence of the Prandtl number $P_r$. Fig. 4 depicts the influence of the radiation parameter $N_r$ on the temperature distribution of Casson fluid for different values. The graphs reveal that the energy profile increases as the $N_r$ values increase. Physically, as the heat flux changes, it leads to a reduction in $k_1$ along the plate in the normal direction. This indicates that a greater amount of heat radiation is absorbed by the fluid, resulting in an elevated temperature profile.
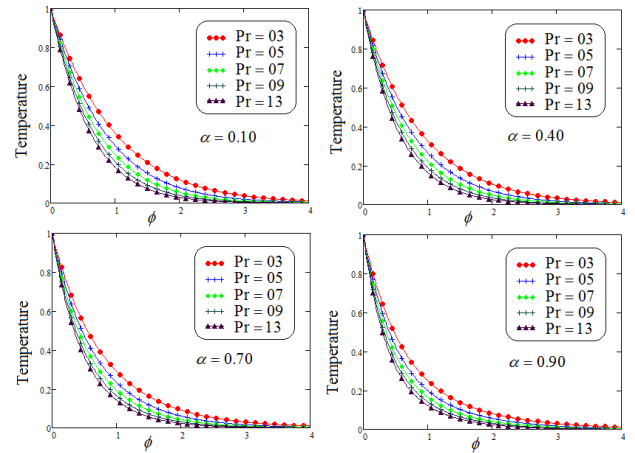


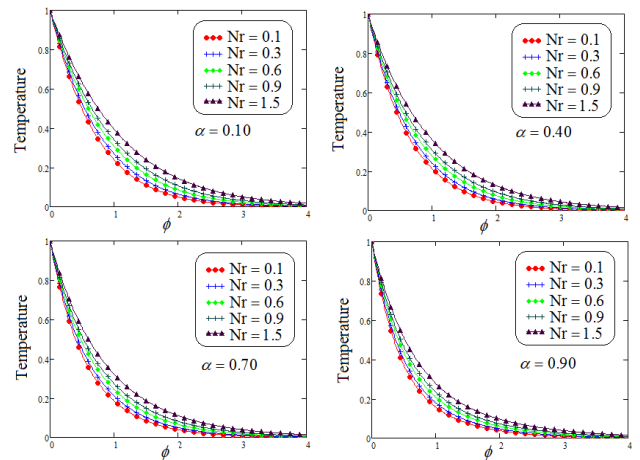**Fig. 3.** Representation of Casson fluid temperature against $\varphi$ for multiple values of $P_r$



**Fig. 4.** Representation of Casson fluid temperature against $\varphi$ for multiple values of $N_r$
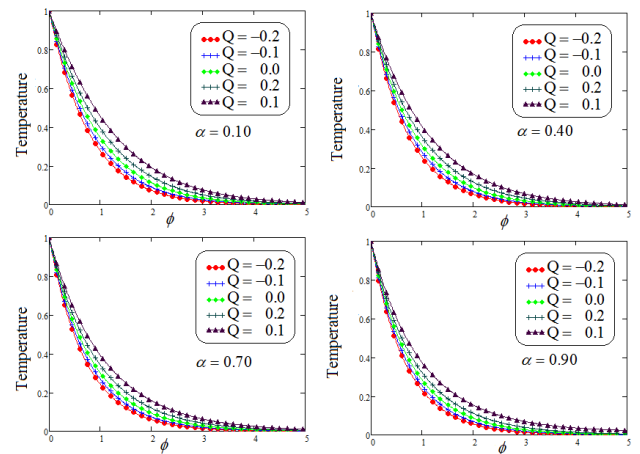


**Fig. 5.** Representation of Casson fluid temperature against $\varphi$ for multiple values of Q

Fig. 5 illustrates the correlation between the quantity of heat, whether extracted ($Q < 0$) or supplied ($Q > 0$), and temperature. It can be observed that the energy profile increases as the values of $Q$ rise, indicating the considerable impact of heat extraction or generation in cooling and heating procedures. Furthermore, Fig. 6 exhibits the influence of parameter $\alpha$ on the fluid

Aziz Ur Rehman, Fahd Jarad, Muhammad Bilal Riaz
*A Fractional Study of MHD Casson Fluid Motion with Thermal Radiative Flux and Heat Injection/Suction Mechanism under Ramped Wall Condition:*
*Application of Rabotnov Exponential Kernel*

DOI 10.2478/ama-2024-0011

flow. The descending velocity curves provide a clear representation of how varying values of $\alpha$ impact the flow behaviour. Fig. 7 describes the influence of the Casson fluid parameter, $\beta$, on the velocity graphs of the Casson fluid in relation to $\varphi$. Various values of $\beta$ were selected to examine the effects on different fluidic parameters.
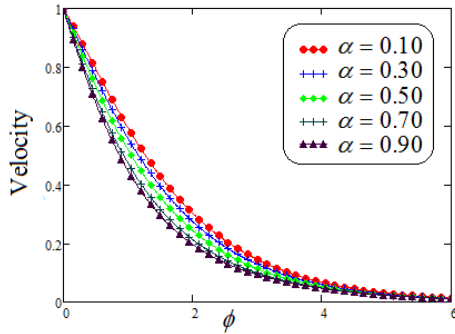


**Fig. 6.** Velocity representation for multiple values of $\alpha$
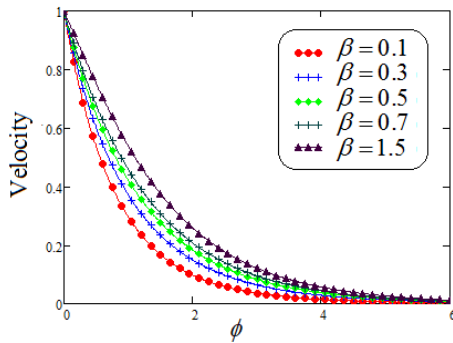


**Fig. 7.** Velocity representation for multiple values of $\beta$

Fig. 8 depicts the effect of the Prandtl number, denoted as $P_r$, on the velocity of Casson fluid as a function of $\varphi$, while considering different values of $P_r$ at four distinct fractional parameter values of $\alpha$. It is noteworthy that the Prandtl number plays a significant role in determining the behaviour of the Casson fluid velocity profile within the boundary layer. As the values of $P_r$ vary, noticeable changes in the velocity distribution within the boundary layer are observed as decay in the boundary layer of velocity noticed corresponding to rise in the distinct values of $P_r$. To provide a more comprehensive understanding of the impact of the Grashof number $G_r$, Fig. 9 has been plotted. The Grashof number represents the ratio between buoyancy force and viscous force. As $G_r$ increases, indicating a higher fraction of buoyancy force compared to viscous force, the fluid velocity experiences a significant boost. This acceleration in fluid velocity is a direct result of the increasing value of $G_r$.

Fig. 10 elucidates the influence of the permeability parameter $K$ on the velocity profiles of the Casson fluid with respect to $\varphi$. Different values of $K$ were chosen to examine the impact of small and large $\alpha$ values. An increase in the porosity of the medium weakens the resistive force, leading to an enhancement in the flow regime due to momentum development. The graph clearly depicts an elevation in the velocity profile as $K$ values increase under ramped conditions.
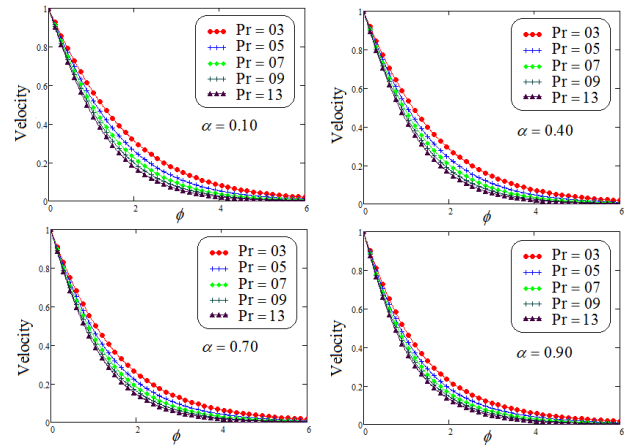


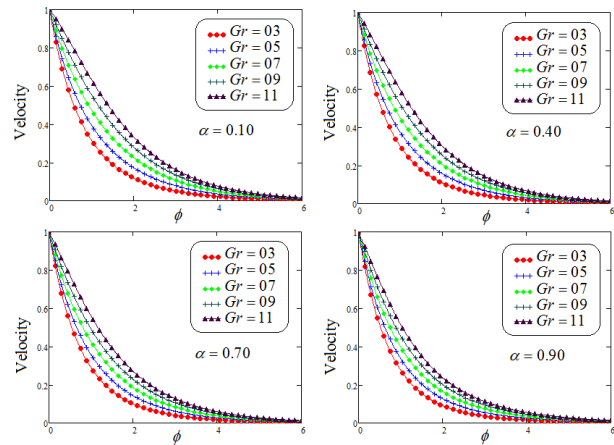**Fig. 8.** Velocity representation for multiple values of $P_r$



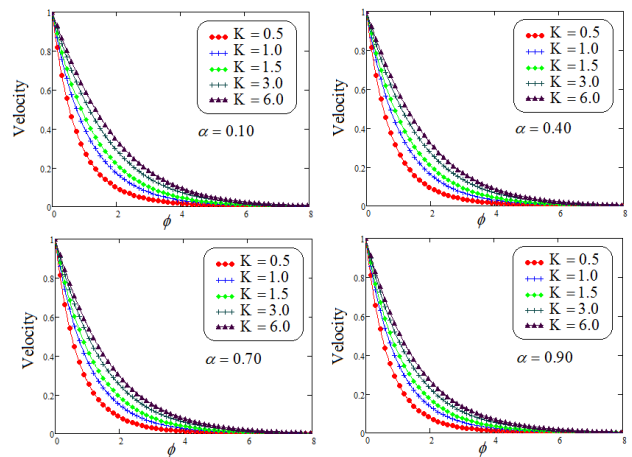**Fig. 9.** Velocity representation for multiple values of $G_r$



**Fig. 10.** Velocity representation for multiple values of $K$

Fig. 11 interprets the influence of the magnetic number $M$ on the momentum profile concerning $\varphi$, by assigning different values of $M$ in the velocity equation. This visualization aims to demonstrate the physical behaviour of the velocity of Casson fluid corresponding to various fractional parameter values. The results show that both the magnitude of the boundary layer thickness and the

velocity decrease when a strong magnetic field is applied. Consequently, this observation indicates that the fluid experiences a slow down as the magnetic number increases, as the dragging forces dominate over the flow-supporting forces. Ultimately, the velocity contour diminishes as the magnetic number values increase.
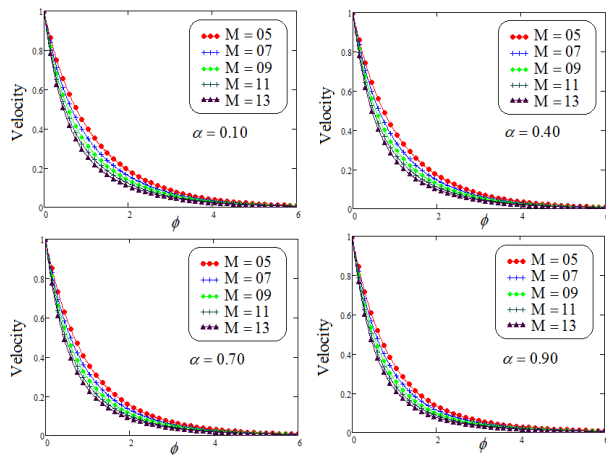


**Fig. 11.** Velocity representation for multiple values of $M$

## 6. CONCLUSION

This research article aims to explore the behaviour of MHD natural convective flow of Casson fluid, a type of non-Newtonian fluid, by obtaining analytical solutions using the non-integer-order derivative known as YAC. The study focuses on the fluid flow in the vicinity of an infinitely vertical plate. To analyse the system of equations governing the flow, the LT technique is employed. This mathematical tool helps in transforming the equations into a different domain, where they can be solved more effectively. By applying the LT to the fractional system of equations, the researchers are able to derive solutions in a series form, which provides a mathematical representation of the behaviour of the Casson fluid under MHD natural convective flow conditions. Furthermore, the obtained solutions are presented using special functions, which are mathematical functions that have specific properties and are commonly used to describe complex phenomena. The use of special functions allows for a more concise and precise representation of the results. The researchers analyse the graphical behaviour of the solutions to gain insights into the characteristics of the Casson fluid flow. These graphical representations provide valuable information about various aspects of the flow, such as velocity profiles and heat distribution. By observing the trends and patterns in the graphs, important key points can be identified and expressed as follows:

– With an increase in the memory parameter $\alpha$, the velocity field and temperature experience a gradual decrease. In other words, higher values of $\alpha$ result in lower velocities and temperatures.
– When the Prandtl number $P_r$ increases, it indicates a higher ratio of momentum diffusivity to thermal diffusivity in a fluid. In practical terms, this means that the fluid is more efficient at transferring momentum than heat. As a result, both the velocity field and temperature exhibit a decreasing trend.
– As the values of the parameters $N_r$ and $Q$ increase, the effect on the temperature profile becomes more pronounced.

A higher $N_r$ implies a greater influence of radiation, leading to elevated temperatures. Similarly, an increase in the heat injection/suction parameter $Q$ amplifies the impact on the temperature distribution, resulting in higher temperatures.

– Elevated values of the parameters $G_r$ and $K$ have a positive effect on the velocity of the Casson fluid, resulting in an increase in its flow speed. The larger the values of $G_r$ and $K$, the greater the enhancement observed in the velocity of the Casson fluid.
– When the magnetic number $M$ increases, the impact of magnetic forces on the fluid becomes more significant. This increased influence results in a reduction in the fluid velocity. The magnetic forces act as a resistance, impeding the fluid flow and causing a decrease in velocity as the magnetic number increases.

## REFERENCES

1. Kahshan M, Lu D, Siddiqui AM. A Jeffrey fluid model for a porous-walled channel: Application to flat plate dialyzer, Sci. Rep. 2019;9(1):1-18.
2. Mohebbi R, Delouei AA, Jamali A, Izadi M, Mohamad AA. Pore-scale simulation of non-Newtonian power-law fluid flow and forced convection in partially porous media: Thermal lattice Boltzmann method, Physica A. 2019; 525: 642-656.
3. Riaz MB, Rehman AU, Wojciechowski A, Atangana A. Heat and mass flux analysis of magneto-free-convection flow of Oldroyd-B fluid through porous layered inclined plate. Sci Rep. 2023;13: 653. https://doi.org/10.1038/s41598-022-27265-w
4. Riaz MB, Abro KA, Abualnaja KM. Akgül A. Rehman AU, Abbas M, Hamed YS. Exact solutions involving special functions for unsteady convective flow of magnetohydrodynamic second grade fluid with ramped conditions, Advances in Difference Equations. 2021; 408. https://doi.org/10.1186/s13662-021-03562-y
5. Riaz MB, Awrejcewicz J, Rehman AU. Functional Effects of Permeability on Oldroyd-B Fluid under Magnetization: A Comparison of Slipping and Non-Slipping Solutions. Appl. Sci. 2021; 11: 11477 https://doi.org/10.3390/app112311477.
6. Khan Z, Tairan N, Mashwani WK, Rasheed HU, Shah ., Khan W. MHD and slip effect on two-immiscible third grade fluid on thin film flow over a vertical moving belt, Open Phys. 2019; 17 (1); 575-586.
7. Casso N. A flow equation for pigment-oil suspensions of the printing ink type. In Rheology of Disperse Systems. Ed. Mill, C. C. Pergamon Press, Oxford. 1959; 84-104.
8. Hussain M, Ali A, Ghaffar A. et al. Flow and thermal study of MHD Casson fluid past a moving stretching porous wedge. J Therm Anal Calorim.2022;147:6959-6969.
https://doi.org/10.1007/s10973-021-10983-0
9. Hussain M, Ghaffar A, Ali A, Shahzad A, Nisar KS, Alharthi MR, Jamshed W. MHD thermal boundary layer flow of a Casson fluid over a penetrable stretching wedge in the existence of nonlinear radiation and convective boundary condition, Alexandria Engineering Journal.2021;60(6):5473—5483. https://doi.org/10.1016/j.aej.2021.03.042
10. Ali A, Hussain M, Anwar MS. et al. Mathematical modeling and parametric investigation of blood flow through a stenosis artery. Appl. Math. Mech.-Engl. Ed.2021; 42:1675-1684.
https://doi.org/10.1007/s10483-021-2791-8
11. Khalid A, Khan I, Khan A, Shafie S. Unsteady MHD free convection flow of Casson fluid past over an oscillating vertical plate embedded in a porous medium. Eng. Sci. Technol. Int. J. 2015;18(3):309-317.
12. Hussain M, Ali A, Inc M, Sene N, Hussan M. Impacts of Chemical Reaction and Suction/Injection on the Mixed Convective Williamson Fluid past a Penetrable Porous Wedge, Journal of Mathematics. 2022. https://doi.org/10.1155/2022/3233964
13. Bhattacharyya K, Hayat T, Alsaedi A. Analytic solution for magnetohydrodynamic boundary layer flow of Casson fluid over a stretch-

ing/shrinking sheet with wall mass transfer. Chin. Phys. B. 2013;22(2): 024702.

14. Oka S. An approach to $\alpha$ unified theory of the flow behavior of time-independent non-Newtonian suspensions. Jpn. J. Appl. Phys.1971; 10(3): 287.

15. Riaz MB, Awrejcewicz J Rehman AU, Abbas M. Special functions-based solutions of unsteady convective flow of a MHD Maxwell fluid for ramped wall temperature and velocity with concentration. Advances in Difference Equations 2021.
https://doi.org/10.1186/s13662-021-03657-6

16. Hussain Z, Alshomrani AS. Muhammad T, Anwar MS. Entropy analysis in mixed convective flow of hybrid nanofluid subject to melting heat and chemical reactions, Case Studies in Thermal Engineering.2022;34. https://doi.org/10.1016/j.csite.2022.101972.

17. Mernone AV, Mazumdar JN, Lucas SK. A mathematical study of peristaltic transport of a Casson fluid. Math. Comput. Model. 2002; 35(7-8): 895-912.

18. Arthur EM, Seini IY, Bortteir B. Analysis of Casson fluid flow over a vertical porous surface with chemical reaction in the presence of magnetic field. J Appl. Math. Phys. 2015;3:713-723.

19. Mukhopadhyay S. Effects of thermal radiation on Casson fluid flow and heat transfer over an unsteady stretching surface subjected to suction/blowing. Chin. Phys. B.2013;22(11): 114702.

20. Mustafa M, Hayat T, Pop I, Aziz A. Unsteady boundary layer flow of a Casson fluid due to an impulsively started moving flat plate. Heat Transf. 2011;40(6): 563-576.

21. Rehman AU, Riaz MB, Khan I, Mohamed A. Time fractional analysis of Casson fluid with application of novel hybrid fractional derivative operator. AIMS Mathematics, 2023; 8(4): 8185-8209.
https://doi.org/10.3934/math.2023414.

22. Riaz MB, Rehman AU Awrejcewicz J Akgül A. Power Law Kernel Analysis of MHD Maxwell Fluid with Ramped Boundary Conditions: Transport Phenomena Solutions Based on Special Functions. Fractal Fract.2021;5:248. https://doi.org/10.3390/fractalfract5040248.

23. Rehman AU, Riaz MB, Rehman W, Awrejcewicz J, Baleanu D. Fractional Modeling of Viscous Fluid over a Moveable Inclined Plate Subject to Exponential Heating with Singular and Non-Singular Kernels. Math. Comput. Appl. 2022; 27: 8.
https://doi.org/10.3390/mca27010008

24. Kumar S, Ghosh S, Samet B, Doungmo Goufo EF. An analysis for heat equations arises in diffusion process using new Yang-Abdel-Aty-Cattani fractional operator. Mathematical Methods in the Applied Sciences.2020;43(9):6062-6080. https://doi.org/10.1002/mma.6347.

25. Bagley RL, Torvik PJ. A theoretical basis for the application of fractional calculus to viscoelasticity, J. Rheol. 1983; 27 (3): 201-210.

26. Rehman AU, Riaz MB, Atangana A, Jarad F, Awrejcewicz J. Thermal and concentration diffusion impacts on MHD Maxwell fluid: A generalized Fourier's and Fick's perspective, Case Studies in Thermal Engineering.2022;35. https://doi.org/10.1016/j.csite.2022.102103

27. Riaz MB, Awrejcewicz J, Rehman AU, Akgül A. Thermophysical Investigation of Oldroyd-B Fluid with Functional Effects of Permeability: Memory Effect Study Using Non-Singular Kernel Derivative Approach. Fractal Fract. 2021; 5: 124.
https://doi.org/10.3390/fractalfract5030124

28. Rehman AU, Jarad F, Riaz MB, Shah ZH. Generalized Mittag-Leffler Kernel Form Solutions of Free Convection Heat and Mass Transfer Flow of Maxwell Fluid with Newtonian Heating: Prabhakar Fractional Derivative Approach. Fractal Fract. 2022; 6: 98.
https://doi.org/10.3390/fractalfract6020098.

29. Mohammadi H, Kumar S, Rezapour S, Etemad S. A theoretical study of the Caputo–Fabrizio fractional modeling for hearing loss due to Mumps virus with optimal control. Chaos, Solitons & Fractals.2021; 144. https://doi.org/10.1016/j.chaos.2021.110668.

30. Rehman AU, Riaz MB, Wojciechowski A. Thermo diffusion impacts on the flow of second grade fluid with application of (ABC), (CF) and (CPC) subject to exponential heating. Sci Rep. 2022; 12:18437
https://doi.org/10.1038/s41598-022-21773-5.

31. Kumar S, Nisar KS, Kumar R, Cattani C, Samet B. A new Rabotnov fractional-exponential function-based fractional derivative for diffusion equation under external force. Mathematical Methods in the Applied Sciences. 2020; 43(7): 4460-4471. https://doi.org/10.1002/mma.6208

32. Jleli M, Kumar S, Kumar R, Samet B. Analytical approach for time fractional wave equations in the sense of Yang-Abdel-Aty-Cattani via the homotopy perturbation transform method, Alexandria Engineering Journal. 2020; 59(5): 2859-2863.
https://doi.org/10.1016/j.aej.2019.12.022

33. Hayat T, Sajjad R, Asghar S. Series solution for MHD channel flow of a Jeffery fluid, Commun. Nonlin. Sci. Numer. Simulat. 2010; 15(9):2400-2406. https://doi.org/10.1016/j.cnsns.2009.09.033.

34. Kumar S, Chauhan RP. Momani S., Hadid S. Numerical investigations on COVID-19 model through singular and non-singular fractional operators. Numerical Methods for Partial Differential Equations. https://doi.org/10.1002/num.22707.

35. Rehman AU, Riaz MB., Saeed ST, Jarad F, Jasim H N., Enver A. An Exact and Comparative Analysis of MHD Free Convection Flow of Water-Based Nanoparticles via CF Derivative, Mathematical Problems in Engineering. 2022. https://doi.org/10.1155/2022/9977188.

36. Riaz MB, Rehman AU, Awrejcewicz J. Double Diffusive Magneto-Free-Convection Flow of a Maxwell Fluid Over a Vertical Plate: Special Functions Based Analysis using Local and Non-Local Kernels to Heat and Mass Flux subject to Exponential Heating, Fractals. 2022; 30(5). https://doi.org/10.1142/S0218348X22401570.

37. Rehman AU, Riaz MB, Atangana A. Time fractional analysis of Casson fluid with Rabotnov exponential memory based on the generalized Fourier and Fick... s law, Scientific African. 2022;17: e01385, https://doi.org/10.1016/j.sciaf.2022.e01385.

38. Kumar S, Kumar A, Samet B, Dutta H. A study on fractional host–parasitoid population dynamical model to describe insect species. Numerical Methods for Partial Differential Equations. 2021; 37(2): 1673-692. https://doi.org/10.1002/num.22603.

39. Anwar MS, Irfan M, Hussain M, Muhammad T, Hussain Z. Heat Transfer in a Fractional Nanofluid Flow through a Permeable Medium, Mathematical Problems in Engineering.2022.
https://doi.org/10.1155/2022/3390478

40. Anwar T, Kumam P, Watthayu W. Unsteady MHD natural convection flow of Casson fluid incorporating thermal radiative flux and heat injection/suction mechanism under variable wall conditions. Sci Rep. 2021;11: 4275. https://doi.org/10.1038/s41598-021-83691-2.

41. Khalid A, Khan I, Khan A, Shafie S. Unsteady MHD free convection flow of Casson fluid past over an oscillating vertical plate embedded in a porous medium. Eng. Sci. Technol. Int. J. 2015;18(3):309-317

42. Mustafa M, Khan JA. Model for flow of Casson nanofluid past a nonlinearly stretching sheet considering magnetic field effects. AIP Adv. 2015;5(7): 077148.

43. Yang XJ, Abdel-Aty M, Cattani C. A new general fractional order derivative with Rabotnov fractional exponential kernel applied to model the anomalous heat.Thermal Science. 2019; 23(3A): 1677-1681.

Aziz Ur Rehman: [iD] https://orcid.org/0000-0002-8804-3915

Fahd Jarad: [iD] https://orcid.org/0000-0002-3303-0623

Muhammad Bilal Riaz: [iD] https://orcid.org/0000-0001-5153-297X